



HAL
open science

Thermoelectric Properties of Ternary and Quaternary Mo6 and Mo9 Cluster Selenides

Christophe Candolfi, Patrick Gougeon, Philippe Gall, Michel Potel, Anne
Dauscher, Bertrand Lenoir

► **To cite this version:**

Christophe Candolfi, Patrick Gougeon, Philippe Gall, Michel Potel, Anne Dauscher, et al.. Thermoelectric Properties of Ternary and Quaternary Mo6 and Mo9 Cluster Selenides. Jean-François Halet (ed). Ligated Transition Metal Clusters in Solid-state Chemistry, 180, Springer, pp.125-141, 2019, Structure and Bonding, 978-3-030-25124-6. 10.1007/430_2019_36 . hal-02280139

HAL Id: hal-02280139

<https://univ-rennes.hal.science/hal-02280139>

Submitted on 9 Sep 2019

HAL is a multi-disciplinary open access archive for the deposit and dissemination of scientific research documents, whether they are published or not. The documents may come from teaching and research institutions in France or abroad, or from public or private research centers.

L'archive ouverte pluridisciplinaire **HAL**, est destinée au dépôt et à la diffusion de documents scientifiques de niveau recherche, publiés ou non, émanant des établissements d'enseignement et de recherche français ou étrangers, des laboratoires publics ou privés.

Thermoelectric Properties of Ternary and Quaternary Mo₆ and Mo₉ Cluster Selenides

Christophe Candolfi^{*a}, Patrick Gougeon^b, Philippe Gall^b, Michel Potel^b, Anne Dauscher^a,
Bertrand Lenoir^a

^a Institut Jean Lamour, UMR 7198 CNRS – Université de Lorraine, 2 allée André Guinier-
Campus ARTEM, BP 50840, 54011 Nancy Cedex, France

^b Institut des Sciences Chimiques de Rennes, UMR 6226 CNRS – Université de Rennes 1 -
INSA de Rennes, 11 allée de Beaulieu, CS 50837, F-35708 Rennes Cedex, France

*Corresponding author: christophe.candolfi@univ-lorraine.fr

Abstract

Mo-based cluster compounds containing Mo₆ and Mo₉ cluster units have long been known for their rich chemistry and the diversity and complexity of their crystal structures. While most studies have mainly focused on their crystallographic properties, recent investigations have pointed out their potential for thermoelectric applications in power generation. These compounds derive their good properties from the three-dimensional arrangement of the

clusters between which cations reside. This inherent disorder strongly limits the ability of these materials to transport heat that often leads to a temperature dependence of the lattice thermal conductivity that mirrors that observed in glassy systems. In addition, most of these compounds can be driven from a metallic toward a semiconducting state through insertion of additional cations. Here, we review the recent progress made on determining the transport properties of these compounds, discussing in particular the key ingredients that lead to their peculiar thermal properties, and examine possible future directions to further enhance their thermoelectric properties.

Keywords: chalcogenide; cluster; semiconductor; thermal conductivity; thermoelectric

Contents

1. Introduction	3
2. Synthesis and crystal structure	5
2.1 Syntheses and crystal growth	5
2.2 Crystal Structures	8
3. Thermoelectric properties	16
3.1 Electronic properties	16
3.2 Thermal properties	22
4. Conclusion	26
References	28

1. Introduction

Thermoelectric materials in which a temperature difference generates an electric field and vice versa, enable direct solid-state energy conversion between heat and electricity [1-3]. While thermoelectric refrigerators would provide an elegant alternative to replace compression-based refrigerators, thermoelectric generators would allow for a systematic production of electricity from waste-heat sources. The design and optimization of efficient thermoelectric devices is intimately linked to the physical properties of the materials that constitute their active part [1-3]. The conversion efficiency of the device is governed by the so-called dimensionless thermoelectric figure of merit ZT defined at the absolute temperature T as $ZT = \alpha^2 T / \rho \kappa$ where ρ is the electrical resistivity, α is the thermopower (or Seebeck coefficient), and κ is the total thermal conductivity which is the sum of a lattice (κ_L) and an electronic (κ_e) contribution [1-3]. The interdependence of these three transport properties via the carrier concentration makes the optimization of thermoelectric materials a challenging task. Among the various strategies used to identify promising systems, the search for materials that inherently behave as good thermal insulators can be driven by simple guiding rules based on their crystallographic characteristics. A complex unit cell containing a large number of heavy atoms has been traditionally a fruitful guiding principle to discover compounds that exhibit low lattice thermal conductivity values [4-14].

The diversity, flexibility, and complexity of the crystal structures formed by cluster compounds based on molybdenum atoms naturally make these materials worthy of detailed experimental and theoretical investigations. The Chevrel phases $M_x\text{Mo}_6\text{X}_8$ (M = alkali,

alkaline-earth, rare-earth, transition metals; $X = S, Se, \text{ and } Te$; $0 \leq x \leq 4$), the crystal structures of which are based on the octahedral Mo_6 cluster, are one of the most famous family of such compounds widely investigated for their magnetic, superconducting, and thermoelectric properties [15,16]. A remarkable property of their crystal structure is the possibility to accommodate various types of cations in the voids existing between the Mo_6X_8 clusters. These cations provide additional electrons that drive the compound toward a semiconducting state and help to lower the lattice thermal conductivity. From these two combined effects, interesting thermoelectric properties emerge with a peak ZT value of 0.6 at 1150 K achieved in the composition $(Cu/Fe)Mo_6Se_8$ [17].

Clusters with higher nuclearities ($Mo_9, Mo_{12}, Mo_{15}, Mo_{18}, Mo_{21}, Mo_{24}, Mo_{30}, \text{ and } Mo_{36}$ cluster units) have been obtained in more than 40 different structure types and extensively studied over the last decades [18-29]. As in Chevrel phases, various cations can be inserted in the inter-cluster space to stabilize the structure. These voids are significantly larger than those present in the Chevrel phases, often leading to very large, anisotropic thermal displacement parameters for the cations [18-29]. The strong disorder induced by the presence of these intercluster atoms is an important ingredient that helps to limit the propagation of heat-carrying acoustic phonons [30-41].

In this chapter, we provide a brief overview of the results obtained experimentally on the thermoelectric properties of these materials over the last few years. Due to the diversity of structures that can be built with Mo-based clusters, we will focus on compounds that are formed by Mo_6 and Mo_9 cluster units with known transport properties. We will also present the main crystallographic features that give rise to very low, glass-like lattice thermal

conductivity. Our main objective is to highlight the potential of this large class of materials for thermoelectric applications and present possible future directions to further enhance their thermoelectric properties.

2. Synthesis and crystal structure

2.1 Syntheses and crystal growths

Most of the synthetic routes used to prepare polycrystalline samples are based on direct reactions of powders (Mo, Ag) and precursors (MoSe₂, InSe, TlSe) in sealed silica tubes at high temperatures [30-41]. Prior to use, Mo powders are reduced under H₂ flowing gas at 1000°C during 10 h in order to eliminate traces of oxygen. The precursors are also synthesized by direct reaction of elements of high purity in sealed silica tubes. Monophasic powders of MoSe₂, InSe, and TlSe are obtained by heating stoichiometric mixtures of elemental powders at 700, 800, and 500°C, respectively, during 48 h.

For the series Ag_xMo₉Se₁₁ with nominal compositions $x = 3.4, 3.5, 3.75, 3.8, 3.9,$ and 4.0, stoichiometric amounts of MoSe₂, Mo, and Ag in powder form are cold pressed into cylindrical pellets which are subsequently placed in silica tubes sealed under vacuum [30,31,36,37,40]. The tubes are then heated at 950°C for 48 h.

In some cases, a quaternary phase can be obtained by direct reaction of a ternary cluster compound with an excess of another element during long-term annealing at high temperatures. This kind of synthesis has been successfully applied to Tl₂Mo₉Se₁₁ in the presence of Ag powders which led to the formation of the novel quaternary compound

$\text{Ag}_2\text{Tl}_2\text{Mo}_9\text{Se}_{11}$ after annealing at 800°C during two weeks [32]. Subsequent syntheses of polycrystalline samples of nominal compositions $\text{Ag}_x\text{Tl}_{4-x}\text{Mo}_9\text{Se}_{11}$ ($1.9 \leq x \leq 2.3$) by heating stoichiometric mixtures of Ag, TlSe, MoSe₂, and Mo at 1180°C for 48 hours in evacuated silica tubes evidenced the possibility to vary the Ag-to-Tl ratio while maintaining the monophasic nature of the sample.

The quaternary cluster compound $\text{Ag}_3\text{RbMo}_9\text{Se}_{11}$ has also been discovered following a similar annealing treatment [38]. Reactions of MoSe₂, Ag, and Mo powders mixed with powders of the ternary compound $\text{Rb}_2\text{Mo}_6\text{Se}_6$ at 1200°C for 48 h in sealed silica tubes led to the formation of a phase-pure polycrystalline sample of $\text{Ag}_3\text{RbMo}_9\text{Se}_{11}$. Further experiments revealed that the Ag content can be slightly decreased down to 2.6 atoms per formula unit.

For the $\text{Ag}_3\text{In}_2\text{Mo}_{15}\text{Se}_{19}$ and $\text{Ag}_3\text{Tl}_2\text{Mo}_{15}\text{Se}_{19}$ compounds [33,41], direct reactions of the precursors InSe, TlSe, and MoSe₂ together with Mo and Ag powders have been realized at 1300°C for 40 h. Due to the high temperature required for these reactions, the mixtures were sealed in molybdenum crucibles under a low argon pressure (c.a. 0.6 bar) using an arc welding system.

Some Mo-based cluster compounds cannot, however, be obtained via direct reactions of elements with precursors. This is, for instance, the case of the above-mentioned ternary compound $\text{Rb}_2\text{Mo}_6\text{Se}_6$ used as a precursor [38]. In such a case, a two-step synthesis needs to be considered that notably includes an ion-exchange reaction. As a first step, the ternary compound $\text{In}_2\text{Mo}_6\text{Se}_6$ has been synthesized by heating a stoichiometric mixture of InSe, MoSe₂, and Mo powders at 1000°C during 36 h in a sealed silica tube. The second step then consists in an ion-exchange reaction of $\text{In}_2\text{Mo}_6\text{Se}_6$ with RbCl at 800°C . For this reaction,

$\text{In}_2\text{Mo}_6\text{Se}_6$ and RbCl powders are mixed in the proportion 1:2.5 and cold pressed into a cylindrical pellet which is placed in a long silica tube sealed under vacuum. The end of the ampule where the pellet is located is introduced in a furnace, heated at 800°C during 2 days while maintaining the other end of the tube at room temperature.

The growth of single crystals of these various compounds could be realized by either a vapor-transport technique or by a recrystallization process by subjecting the polycrystalline pellets to an annealing treatment at very high temperature [31-33,38,41]. The former technique has been considered to grow single crystals of $\text{Ag}_3\text{Mo}_9\text{Se}_{11}$ using AgCl as the transport agent in a sealed silica tube [31]. A temperature gradient of 30°C has been applied between both ends of the tubes kept at 1030 and 1060°C during 10 days. The later route has been used to obtain single crystals of the cluster compounds $\text{Ag}_3\text{RbMo}_9\text{Se}_{11}$ [38], $\text{Ag}_3\text{In}_2\text{Mo}_{15}\text{Se}_{19}$ [33], and $\text{Ag}_3\text{Tl}_2\text{Mo}_{15}\text{Se}_{19}$ [41]. While single crystals of $\text{Ag}_3\text{RbMo}_9\text{Se}_{11}$ were obtained by prolonged annealing at 1250°C for 96 h, single crystals of $\text{Ag}_3\text{In}_2\text{Mo}_{15}\text{Se}_{19}$ and $\text{Ag}_3\text{Tl}_2\text{Mo}_{15}\text{Se}_{19}$ could be grown by heating cold-pressed pellets in molybdenum crucibles at 1650°C during 3h with applied heating and cooling rates of 300°C/h and 100°C/h , respectively.

2.2 Crystal structures

The $\text{Ag}_x\text{Mo}_9\text{Se}_{11}$ ($3.4 \leq x \leq 3.9$) compounds crystallize in the orthorhombic space group $Cmcm$ [30,31,36,37,40,42]. The building block of the crystal structure of these compounds is the $\text{Mo}_9\text{Se}_{11}\text{Se}_6$ cluster unit (Figure 1a), which can be seen as the fusion of two octahedral $\text{Mo}_6\text{Se}_8\text{Se}_6$ cluster units (Figure 1b) similar to those found in the Chevrel phases [42].

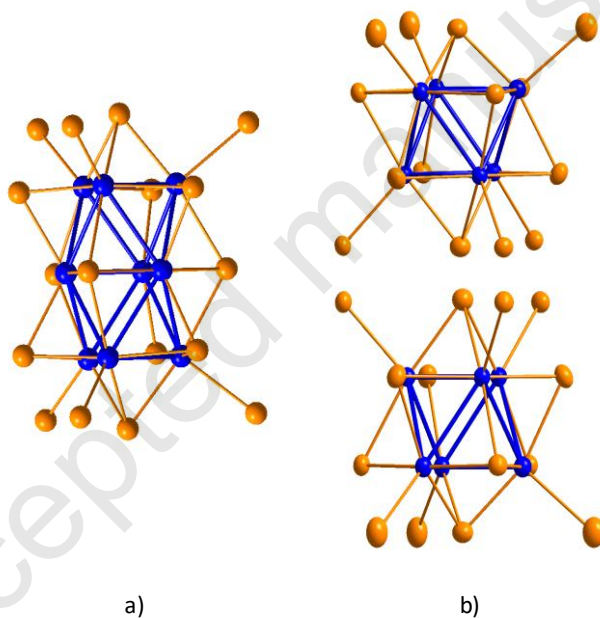


Fig. 1 Schematic representation of the formation of the $\text{Mo}_9\text{Se}_{11}\text{Se}_6$ cluster unit (a) resulting from the condensation of two octahedral $\text{Mo}_6\text{Se}_8\text{Se}_6$ cluster units (b). The Mo and Se atoms are represented in blue and orange, respectively. In both figures, the thermal ellipsoids are represented at the 97% probability level.

The $\text{Mo}_9\text{Se}_{11}\text{Se}_6$ units of point group symmetry C_{2v} or $mmm2$ then share a part of the Se atoms to form the $\text{Mo}_9\text{Se}_{11}$ network. In this arrangement, each of the $\text{Mo}_9\text{Se}_{11}\text{Se}_6$ unit is surrounded by eight other $\text{Mo}_9\text{Se}_{11}\text{Se}_6$ units. This structural arrangement differs from that of the Chevrel phases for which each of the $\text{Mo}_6\text{X}_8\text{X}_6$ unit is only surrounded by six other units. While in the c direction the interconnection between the $\text{Mo}_9\text{Se}_{11}\text{Se}_6$ units is similar to that observed in the Chevrel phases (*i.e.*, each $\text{Mo}_9\text{Se}_{11}\text{Se}_6$ shares eight Mo-Se or Se-Mo interunit bonds; see Figure 2), only four Mo-Se or Se-Mo interunit bonds occur along the b direction (Figure 2). Consequently, the crystal structure of $\text{Ag}_x\text{Mo}_9\text{Se}_{11}$ presents a pseudo-bidimensional character as reflected by the inter-cluster distance of 3.728 Å in the (ac) plane and 4.960 Å in the b direction. The Ag atoms are delocalized over four independent sites. The Ag non-stoichiometry in these compounds arises essentially from the filling of the Ag4 site (shown in dark gray in Figure 2) located in rhomboid cross-sectional channels running along the a direction. The occupation of this site varies from 10 (in $\text{Ag}_{3.4}\text{Mo}_9\text{Se}_{11}$) up to 25 % (in $\text{Ag}_4\text{Mo}_9\text{Se}_{11}$).

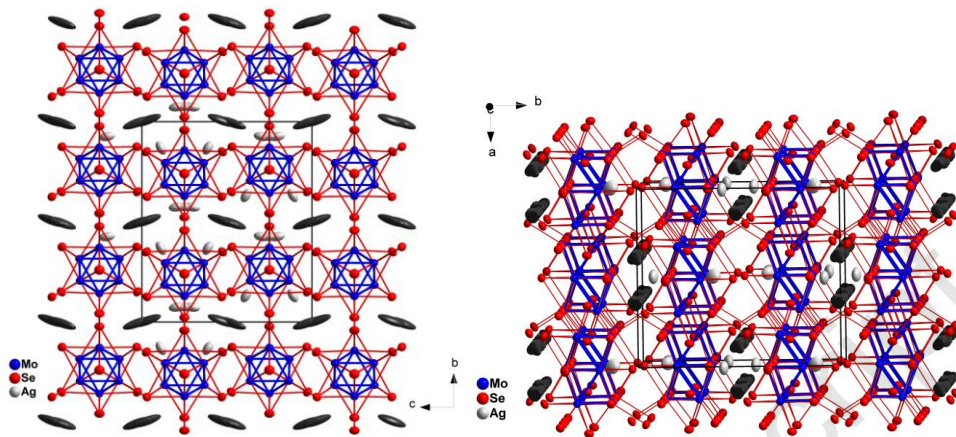


Fig. 2 Projection of the crystal structure of the $\text{Ag}_x\text{Mo}_9\text{Se}_{11}$ compounds (space group $Cmcm$, No. 63) in ellipsoid representation (97% probability level) along the a axis (left) and c axis (right). The Ag, Mo and Se atoms are in gray, blue, and red, respectively. The Ag4 atoms are distinguished from the other Ag atoms by their dark gray color.

While partial substitutions of Cu, Cs, or Cl for Ag and Te and S for Se have been successfully realized and left unchanged the orthorhombic symmetry of the unit cell [36,37,43], other substitutions such as Tl and Rb for Ag result in a different arrangement of the $\text{Mo}_9\text{Se}_{11}\text{Se}_6$ cluster unit [32,38]. Hence, the crystal structures of the quaternary compounds $\text{Ag}_2\text{Tl}_2\text{Mo}_9\text{Se}_{11}$ and $\text{Ag}_3\text{RbMo}_9\text{Se}_{11}$ are described in the space groups $R-3c$ and $P6_3/m$, respectively.

The crystal structure of $\text{Ag}_2\text{Tl}_2\text{Mo}_9\text{Se}_{11}$ consists in a three-dimensional framework formed by interconnected $\text{Mo}_9\text{Se}_{11}\text{Se}_6$ clusters as illustrated in Figure 3 [32].

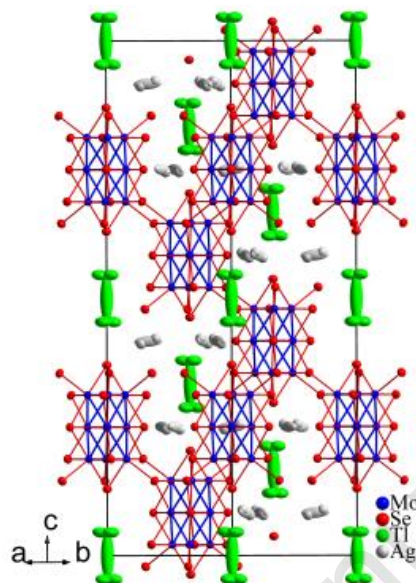


Fig. 3 Perspective view of the crystal structure of $\text{Ag}_2\text{Tl}_2\text{Mo}_9\text{Se}_{11}$ (space group $R\text{-}3c$, No. 167) in ellipsoid representation (97% probability level). The Ag, Tl, Mo, and Se atoms are in light gray, green, blue, and red, respectively.

The $\text{Mo}_9\text{Se}_{11}\text{Se}_6$ unit has here the point symmetry 32 or D_3 . The outer and inner atoms display different environments. The environment of the former is similar to that encountered in the $\text{Mo}_6\text{X}_8\text{X}_6$ units ($X = \text{S}, \text{Se}$) of the Chevrel phases. They are surrounded by four Mo atoms and four Se atoms, in an approximately coplanar coordination, with another Se atom belonging to an adjacent $\text{Mo}_9\text{Se}_{11}$ cluster. This last atom constitutes the apex of a square-based pyramidal environment. The Mo atoms of the median Mo_3 triangles are surrounded by six Mo and only four Se atoms belonging to the same cluster unit. The Mo-

Mo distances range from 2.62 up to 2.75 Å. The Mo-Se bond distances are typical, ranging between 2.56 Å and 2.67 Å. Each unit is connected to six adjacent units via 12 interunit Mo-Se bonds of 2.66 Å to form a three-dimensional Mo-Se framework with the connective formula $[\text{Mo}_9\text{Se}_5^i\text{Se}_{6/2^{i-a}}]\text{Se}_{6/2^{a-i}}$ according to Schäfer's notation and in which the shortest intercluster distance is 3.69 Å. While the Ag atoms occupy a distorted trigonal bipyramidal site formed by the Se atoms, the Tl atoms occupy sites of ten Se atoms forming a distorted tetrahedron. The three faces of these tetrahedra are capped with three edges bridged with Tl-Se distances in the range 3.02 - 4.38 Å or surrounded by 6 Se atoms at 3.40 Å forming a trigonal antiprism.

The Mo-Se network of the $\text{Ag}_3\text{RbMo}_9\text{Se}_{11}$ compound [38] also originates from interlinked $\text{Mo}_9\text{Se}_{11}\text{Se}_6$ clusters via Mo-Se bonds (Figure 4). The $\text{Mo}_9\text{Se}_{11}$ unit has the point symmetry C_{3h} . The connective formula of the molybdenum-selenium framework is $[\text{Mo}_9\text{Se}_5^i\text{Se}_{6/2^{i-a}}]\text{Se}_{6/2^{a-i}}$ according to the notation of Schäfer.²⁸

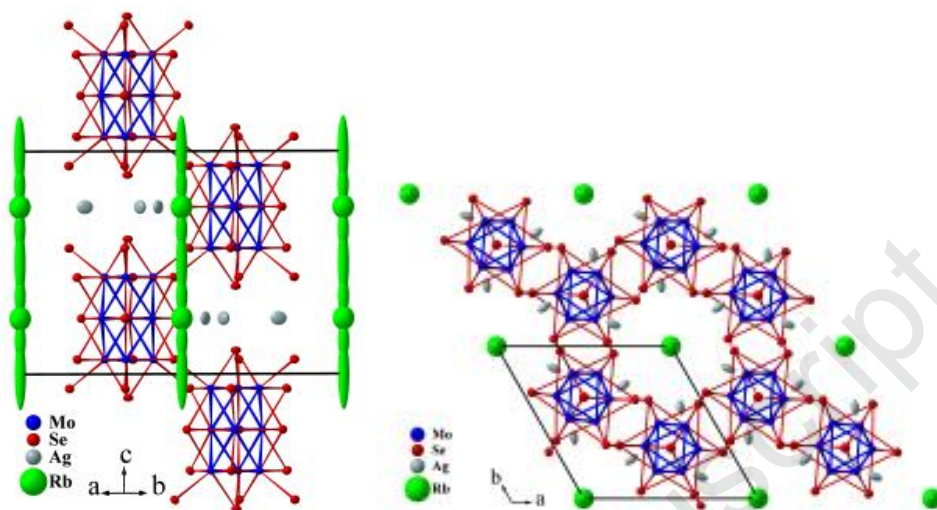


Fig. 4 (Left) Perspective view of the crystal structure of $\text{Ag}_2\text{Tl}_2\text{Mo}_9\text{Se}_{11}$ (space group $P6_3/m$, No. 176) in ellipsoid representation (97% probability level). (Right) Projection of the crystal structure onto the (ab) plane. The Ag, Rb, Mo, and Se atoms are in light gray, green, blue, and red, respectively.

As shown in Figure 4, which shows the crystal structure of $\text{Ag}_3\text{RbMo}_9\text{Se}_{11}$ projected onto the (ab) plane, large hexagonal tunnels that are randomly filled by the Rb^+ cations run along the c axis. The Ag^+ cations partially occupy positions in the mirror planes around the ternary axes between adjacent $\text{Mo}_9\text{Se}_{11}\text{Se}_6$ units located on the three-fold axis. The Se environment of Ag atoms can be seen as a distorted square pyramid with Ag-Se bond lengths ranging from 2.64 to 2.93 Å. One of the Rb cations resides in distorted tri-capped trigonal prismatic Se environment, while the other ones are each surrounded by six Se atoms forming flattened

octahedra along the ternary axis. The Rb-Se distances spread over a wide range of 3.41 – 3.99 Å.

The Mo-Se framework of the $\text{Ag}_3\text{M}_2\text{Mo}_{15}\text{Se}_{19}$ ($M = \text{In}, \text{Tl}$) compounds [33,41] is similar to that of $\text{In}_2\text{Mo}_{15}\text{Se}_{19}$ which was the first compound in which the Mo_9 clusters were observed in 1980 [44] (Figure 5).

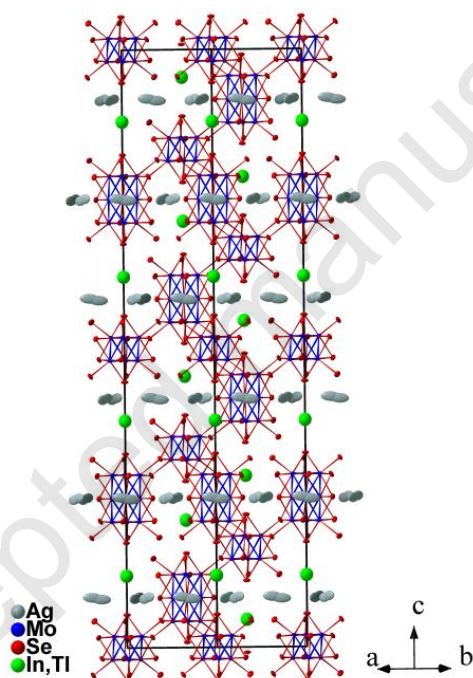


Fig. 5 Perspective view of the crystal structure of $\text{Ag}_3\text{M}_2\text{Mo}_{15}\text{Se}_{19}$ with $M = \text{In}$ or Tl (space group $R\bar{3}c$, No. 167) in ellipsoid representation (97% probability level). The Ag, M, Mo, and Se atoms are in light gray, green, blue, and red, respectively.

Consequently, the crystal structure of these quaternary compounds is based on an equal mixture of $\text{Mo}_6\text{Se}_8^i\text{Se}_6^a$ and $\text{Mo}_9\text{Se}_{11}^i\text{Se}_6^a$ cluster units interconnected through Mo-Se bonds. The first unit can be described as a Mo_6 octahedron surrounded by eight face-capping inner Se^i and six apical Se^a ligands and is identical to that encountered in the Chevrel phases. The second unit is similar to those observed in the three above-mentioned compounds. The $\text{Mo}_6\text{Se}_8^i\text{Se}_6^a$ and $\text{Mo}_9\text{Se}_{11}^i\text{Se}_6^a$ units are centered at the $6b$ and $6a$ positions with the point-group symmetry -3 and 32 , respectively. The Mo-Mo distances within the Mo_6 clusters are about 2.67 \AA for the intra-triangle distances (distances within the Mo_3 triangles formed by the Mo atoms related through the three-fold axis) and 2.70 \AA for the inter-triangle distances. The Mo-Mo distances within the Mo_9 clusters are around 2.65 and 2.74 \AA for the intra-triangle distances and 2.68 and 2.78 \AA for the distances between the triangles. The Mo-Se distances range between 2.57 and 2.63 \AA within the $\text{Mo}_6\text{Se}_8^i\text{Se}_6^a$ unit and between 2.54 and 2.70 \AA within the $\text{Mo}_9\text{Se}_{11}^i\text{Se}_6^a$ unit, as usual. The three-dimensional packing arises from the interconnection of the $\text{Mo}_6\text{Se}_8^i\text{Se}_6^a$ and $\text{Mo}_9\text{Se}_{11}^i\text{Se}_6^a$ cluster units through Mo-Se bonds with each $\text{Mo}_6\text{Se}_8^i\text{Se}_6^a$ unit interconnected to 6 $\text{Mo}_9\text{Se}_{11}^i\text{Se}_6^a$ units (and vice-versa) via Mo-Se interunit bonds. Because of this arrangement, the shortest distance between the Mo_6 and Mo_9 clusters is of the order of 3.60 \AA , indicating only weak metal-metal interaction. In these structures, the Ag atoms occupy distorted triangular bipyramid sites located between two consecutive M sites with Ag-Se distances ranging from 2.58 to 2.88 \AA . The In and Tl atoms are surrounded by seven Se atoms forming a monocapped octahedron compressed along the three-fold axis (see Figure 5).

One common feature of these various crystal structures relevant to understanding their thermal properties is the large, anisotropic thermal displacement parameters (ADPs) of the cations located in the intercluster spaces [30-41]. The largest thermal ellipsoids are observed for the Rb and Tl atoms in the $\text{Ag}_3\text{RbMo}_9\text{Se}_{11}$ and $\text{Ag}_2\text{Tl}_2\text{Mo}_9\text{Se}_{11}$ compounds [32,38], respectively. Low-temperature single-crystal X-ray diffraction measurements performed on $\text{Ag}_2\text{Tl}_2\text{Mo}_9\text{Se}_{11}$ evidenced that the ADP values of the Tl atoms exhibit a nearly temperature-independent behavior down to 85 K [32]. We will see below that the thermal motions of the cations are likely a key ingredient in determining the lattice thermal conductivity.

3. Thermoelectric properties

3.1 Electronic properties

The electronic structure of most of the Mo-based cluster compounds can be deduced from the molecular orbital diagram of the isolated cluster units [27,28,39,43,45-48]. This approach proves to be efficient whenever the clusters in the crystal structure are isolated enough from the neighboring clusters. It has been indeed shown that the interactions between the chalcogen atoms that connect the clusters are not strong enough to perturb the electronic structure of the isolated cluster unit. In such a case, the number of electrons available for metal-metal bonds, called the metallic electron count (MEC), is the critical parameter that determines the metallic or semiconducting nature of the compound.

Semiconducting behavior is predicted to develop when the MEC reaches the optimum value for the cluster unit. In the case of the $\text{Mo}_9\text{Se}_{11}$ clusters, the optimum MEC has been determined to be equal to 36 [46]. Assuming ionic interactions between the cations and the clusters and a +1 valence state for the former, several cations such as Ag, In, Tl, or Rb may thus help to achieve an optimum MEC for the $\text{Mo}_9\text{Se}_{11}$ clusters. Varying the concentration of these cations may also allow for a fine control of the electronic properties by adjusting the carrier concentration.

The thermoelectric potential of materials based on $\text{Mo}_9\text{Se}_{11}$ clusters has been first assessed on the $\text{Ag}_x\text{Mo}_9\text{Se}_{11}$ series [30,31]. Based on the above-mentioned considerations, a semiconducting state is predicted to be reached for $x = 4$. Experimentally, the Ag content can be continuously varied between $x = 3.41$ and $x = 3.81$ leading to a gradual shift from a *p*-type metallic-like behavior ($x = 3.41$) to a *p*-type heavily-doped semiconducting state ($x = 3.81$) (Figure 6) [30,31]. Despite being close to the predicted threshold of $x = 4.0$, the highest Ag content achieved experimentally remains limited to $x = 3.81$. Recent high-resolution fluorescence-detection X-ray absorption spectroscopy (HERFD-XAS) and resonant inelastic X-ray scattering (RIXS) experiments have provided experimental evidence of the presence of subvalent Ag atoms [40], which contribute to limit the electronic properties to a heavily-doped regime. Hence, if the overall effect of Ag on the electronic properties can be fairly well understood by a rigid-band picture, these results nevertheless suggest that the evolution of the electronic structure with x is not entirely captured by this simple picture.

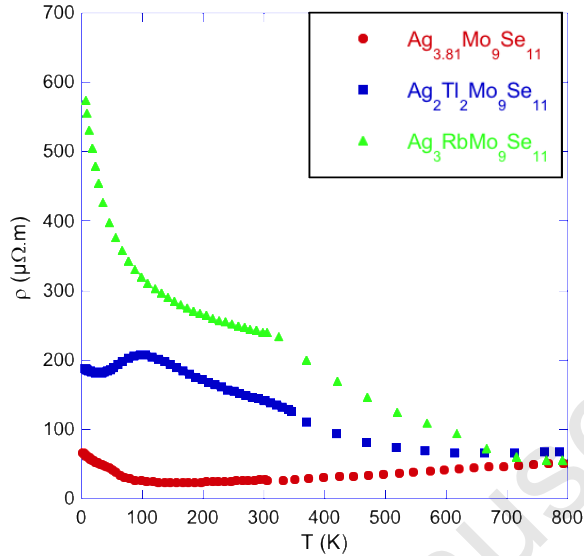


Fig. 6 Comparison of the temperature dependences of the electrical resistivity ρ of

$\text{Ag}_{3.81}\text{Mo}_9\text{Se}_{11}$, $\text{Ag}_2\text{Ti}_2\text{Mo}_9\text{Se}_{11}$, and $\text{Ag}_3\text{RbMo}_9\text{Se}_{11}$.

Although the maximum Ag content accessible is too low to reach a semiconducting behavior, the concomitant increase in the electrical resistivity and thermopower values result in a significant enhancement in the power factor leading to an optimum ZT values of 0.65 at 800 K for $x = 3.81$. This value is higher than the maximum value achieved in the Chevrel phases demonstrating that many of these cluster compounds may show interesting thermoelectric properties at high temperatures.

Attempt at reaching a semiconducting state by insertion of Cu atoms (up to $y = 0.4$) in the $\text{Ag}_{3.6}\text{Mo}_9\text{Se}_{11}$ compound was unsuccessful [37], even though some enhancement in the power factor α^2/ρ has been observed. Further adjustment of the hole concentration in the

$\text{Ag}_x\text{Mo}_9\text{Se}_{11}$ series has been realized through isovalent substitutions and of Te or S for Se [36]. The substitution ranges of these two elements were found to be rather limited with maximum contents of 0.5. These concentrations were too low to significantly influence the transport properties resulting in ZT values comparable to those achieved in unsubstituted samples [31].

Other elements such as Tl and Rb have been considered as possible alternatives to provide the missing charges to the $\text{Mo}_9\text{Se}_{11}$ cluster unit. The addition of Tl and Rb cations in the crystal structure has been successful, giving rise to two new cluster compounds of chemical compositions $\text{Ag}_2\text{Tl}_2\text{Mo}_9\text{Se}_{11}$ and $\text{Ag}_3\text{RbMo}_9\text{Se}_{11}$ [32,38]. As mentioned above, these partial substitutions are accompanied by a change in the lattice symmetry from orthorhombic to hexagonal due to a different arrangement of the $\text{Mo}_9\text{Se}_{11}$ cluster units. Based on their respective chemical compositions, both compounds are predicted to be semiconducting (*i.e.*, 36 electrons per Mo_9) if Ag, Rb, and Tl are monovalent. Unlike the $\text{Ag}_x\text{Mo}_9\text{Se}_{11}$ compounds, this prediction has been verified experimentally with an electrical resistivity following a semiconducting-like temperature dependence (see Figure 5). These results suggest that the specific arrangement of the cluster unit can play an important role in determining the electronic properties of these compounds.

The transport properties of compounds built up from an equal mixture of $\text{Mo}_6\text{Se}_8^i\text{Se}_6^a$ and $\text{Mo}_9\text{Se}_{11}^i\text{Se}_6^a$ cluster units have so far been investigated only on the ternary compound $\text{Rb}_2\text{Mo}_{15}\text{Se}_{19}$ [35] and on the quaternary compounds $\text{Ag}_3\text{In}_2\text{Mo}_{15}\text{Se}_{19}$ and $\text{Ag}_3\text{Tl}_2\text{Mo}_{15}\text{Se}_{19}$ [33,41]. The optimal MEC for the Mo_6Se_8 and $\text{Mo}_9\text{Se}_{11}$ clusters are equal to 24 and 36, respectively, yielding an optimum MEC of 60 for the $\text{Mo}_{15}\text{Se}_{19}$ clusters [33]. Due to the

monovalent character of Rb, the total MEC is equal to 54 in $\text{Rb}_2\text{Mo}_{15}\text{Se}_{19}$ and should thus give rise to *p*-type metallic properties. Measurements of the thermoelectric properties at high temperatures have confirmed this prediction [35]. Further optimization of the thermoelectric properties of $A_2\text{Mo}_{15}\text{Se}_{19}$ compounds implies the introduction of additional charges to bring the MEC closer to 60. Experimentally, this approach can be realized through the insertion of other cations such as Ag or Cu. The two compounds $\text{Ag}_3\text{In}_2\text{Mo}_{15}\text{Se}_{19}$ and $\text{Ag}_3\text{Tl}_2\text{Mo}_{15}\text{Se}_{19}$ provide two examples of such a strategy [33,41]. The presence of Ag helps to achieve heavily-doped semiconducting properties and hence, higher *ZT* values compared to ternary compositions with a peak value of 0.45 at 1100 K in $\text{Ag}_3\text{In}_2\text{Mo}_{15}\text{Se}_{19}$ [33]. The comparison of the electronic properties of both compounds nevertheless indicates that the above-mentioned charge counting scheme is somewhat too simple. The more metallic character of $\text{Ag}_3\text{Tl}_2\text{Mo}_{15}\text{Se}_{19}$ with respect to $\text{Ag}_3\text{In}_2\text{Mo}_{15}\text{Se}_{19}$ promotes the idea that the valence of the cations deviates from the expected +1 value [33,41]. The sensitivity of the transport properties to the nature of the cations should be further investigated by considering other combinations of elements. This might help to determine the important factors behind this behavior, thereby guiding the choice of the most judicious combinations leading to high thermoelectric performances.

One important aspect of the transport in these compounds is the presence of weakly-dispersive valence bands that give rise to electron-like and hole-like contributions to the transport [30-41]. The contributions to the thermopower of these two types of carriers are of opposite sign and thus usually tend to lower the measured values. In spite of this

characteristic, high thermopower values have been nevertheless measured in the compounds containing Mo₉ cluster units (Figure 7).

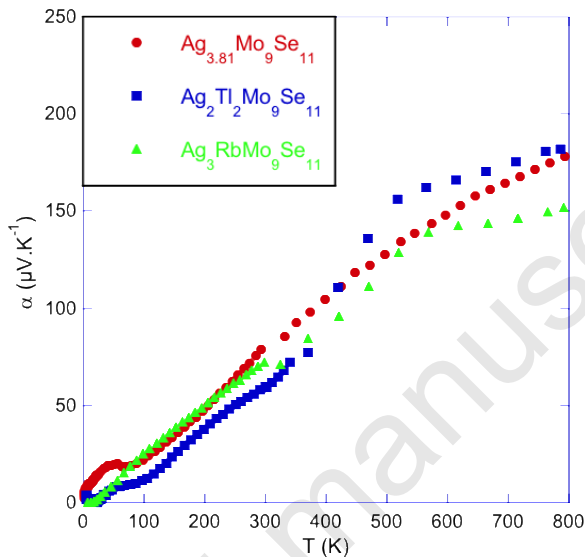


Fig. 7 Comparison of the temperature dependences of the thermopower α of $\text{Ag}_{3.81}\text{Mo}_9\text{Se}_{11}$, $\text{Ag}_2\text{Tl}_2\text{Mo}_9\text{Se}_{11}$, and $\text{Ag}_3\text{RbMo}_9\text{Se}_{11}$.

Direct experimental evidence for multiband transport has been provided by Hall effect measurements at low temperatures. In the $\text{Ag}_x\text{Mo}_9\text{Se}_{11}$ series, the Hall data show a complex behavior as a function of x with a sign change of the Hall coefficient evidenced upon cooling below 200 K [31]. The $\text{Ag}_2\text{Tl}_2\text{Mo}_9\text{Se}_{11}$ compound shows an even more complex behavior with a double sign change of the Hall coefficient upon cooling down to 5 K [32]. These complex temperature dependences make it difficult to determine the actual hole concentration in

these compounds. Another complex evolution of the Hall data has been evidenced in the $\text{Ag}_3\text{In}_2\text{Mo}_{15}\text{Se}_{19}$ compound [33], indicating that the presence of hole-like and electron-like contributions to the transport is neither tied to a particular cluster arrangement, nor to a specific cluster unit. The fact that so far most of the compounds studied exhibit this characteristic suggests that this property may prove to be universal in these materials. It seems therefore natural to ask whether other compounds containing Mo clusters of higher nuclearity may follow this trend or provide a mean to circumvent this problem.

3.2 Thermal properties

One of the distinguishing and common features of these materials is their extremely low lattice thermal conductivity κ that is typically well below $1 \text{ W} \cdot \text{m}^{-1} \cdot \text{K}^{-1}$, with a value of $0.5 \text{ W} \cdot \text{m}^{-1} \cdot \text{K}^{-1}$ often achieved at high temperatures [30,41]. The temperature dependence of κ resembles that observed in amorphous systems, a remarkable physical property for a well-crystallized compound (Figure 8) [49].

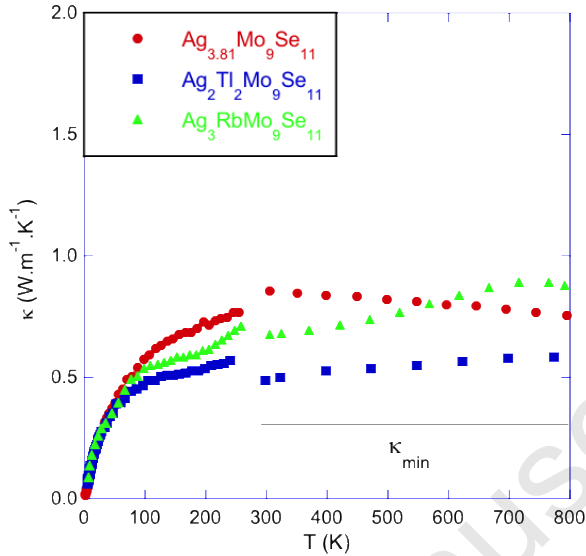


Fig. 8 Comparison of the temperature dependences of the thermal conductivity κ of $\text{Ag}_{3.81}\text{Mo}_9\text{Se}_{11}$, $\text{Ag}_2\text{Tl}_2\text{Mo}_9\text{Se}_{11}$, and $\text{Ag}_3\text{RbMo}_9\text{Se}_{11}$. The horizontal black solid line represents the minimum thermal conductivity ($\sim 0.3 \text{ W} \cdot \text{m}^{-1} \cdot \text{K}^{-1}$) determined by sound velocity measurements. The data between 250 and 300 K have been discarded due to the thermal radiations that accompany low-temperature thermal conductivity measurements.

Several key characteristics of the crystal structure of these compounds likely concur to yield the observed very low, glass-like lattice thermal conductivity. In addition to the large unit cells that result in low phonon cut-off wave vectors [50,51], the large, anisotropic atomic displacement parameters (ADP) values of the cations (Table 1) likely lead to low-lying optical modes that cut the acoustic phonon dispersions. The phase space available for

acoustic phonons is thus strongly reduced resulting in a significant reduction of the lattice thermal conductivity.

Table 1. Largest ADP values for the different cluster compounds determined by single-crystal X-ray diffraction data at 300 K [19,32,33,38,41]. The difference in the stoichiometry of these single crystals and of the polycrystalline compounds is due to the high temperature used during the growth process that leads to a slight loss of Ag.

$\text{Ag}_{3.4}\text{Mo}_9\text{Se}_{11}$	$\text{Ag}_{2.25}\text{Tl}_{1.75}\text{Mo}_9\text{Se}_{11}$	$\text{Ag}_{2.6}\text{RbMo}_9\text{Se}_{11}$	$\text{Ag}_3\text{In}_2\text{Mo}_{15}\text{Se}_{19}$	$\text{Ag}_{2.57}\text{Tl}_2\text{Mo}_{15}\text{Se}_{19}$
Ag ₂	Tl ₂	Rb ₃	Ag	Tl
0.080	0.314	0.28	0.046	0.035

Low-energy optical modes also open an additional channel for Umklapp scattering events which persist down to low temperatures and suppress the dielectric maximum. This mechanism would be then similar to what has been observed in tetrahedrites, for instance, a class of sulfur-based compounds exhibiting similar thermal transport [52,53]. In these minerals, the low-energy optical modes have been shown to be strongly anharmonic [52]. Because anharmonicity determines the scattering probability of phonons during phonon-phonon interactions, highly-anharmonic bonds favor these scattering events and, hence, help to maintain low lattice thermal conductivity upon increasing temperature. This anharmonicity can have several physical origins such as lone pair electrons [52-54], resonant bonds [55], and flat or double-well potentials felt by atoms in cages or tunnels for instance [56-58]. Among these possibilities, the presence of double-well potentials is suggested by the

nearly temperature-independent ADP values observed for the Tl and Rb cations in the $\text{Ag}_2\text{Tl}_2\text{Mo}_9\text{Se}_{11}$ and $\text{Ag}_3\text{RbMo}_9\text{Se}_{11}$ compounds, respectively [32,38]. Similar values have been reported in the type-I clathrates $\text{Sr}_8\text{Ga}_{16}\text{Ge}_{30}$ and $\text{Eu}_8\text{Ga}_{16}\text{Ge}_{30}$ for which, Sr and Eu atoms are off-centered in their cages and can tunnel between potential minima [59-63]. Possible experimental evidence of this behavior in the $\text{Ag}_x\text{Mo}_9\text{Se}_{11}$ series has been obtained by measurements of the specific heat down to 0.35 K [31]. Centered near 1 K, a peak in the lattice contribution to the specific heat when plotted as C_p/T^3 versus T has been evidenced with a magnitude of the peak scaling with the Ag content. While such a peak can be usually well explained via simple models taking into account Einstein-like contributions, the temperature at which this peak is observed is too low to be reasonably accounted for by such models. Thus, this behavior might be due to some of the Ag cations experiencing double-well potentials. More systematic measurements of the low-temperature specific heat of other Mo-based cluster compounds would be worthwhile to determine whether such characteristic is universal in Mo-based cluster compounds.

Although phonon calculations may provide relevant information about the thermal properties of these compounds, the large number of atoms in the unit cell combined with the partial occupancies of the cations makes them highly challenging. It is thus clear that a deeper understanding of the relationships between the key characteristics of the crystal structure and the heat transport will benefit from detailed inelastic neutron and X-ray scattering experiments on both polycrystalline and single-crystalline compounds.

4. Conclusion

Mo-based cluster compounds are a large class of materials in which interesting electronic and thermal phenomena have been evidenced over the last years. The Chevrel phases (based on Mo_6 cluster units) are the most famous representatives of this class where superconductivity, magnetic orders, and thermoelectric properties have been studied in detail since their discovery. Despite compounds built by clusters of higher nuclearity (Mo_9 up to Mo_{36}) are known for several decades, it is not until recently, however, that their transport properties have been studied thoroughly. Their structural complexity is a key characteristic that can potentially result in extremely low lattice thermal conductivity which is one of the prerequisites to make them become potential candidates for thermoelectric applications. Over the last years, several theoretical and experimental studies have revealed that these phases have indeed interesting thermoelectric properties, some of them rivalling with more conventional thermoelectric materials.

While their electronic properties can be often well explained and predicted by simple valence electron counting rules, the microscopic origin of their thermal properties is less well understood. The large thermal displacement parameters of the cations inserted in the inter-cluster voids likely give rise to low-lying optical modes that strongly limit the available phase space for acoustic phonons. The anomalously large ADP values determined in some compounds point to the presence of double-well potentials, as observed in some clathrates, for instance. Further spectroscopic tools such as inelastic neutron scattering studies on both single-crystalline and polycrystalline specimens would be particularly illuminating and

would provide a better understanding of the influence of these characteristics on the heat transport.

Given the large variety of crystal structures that can be synthesized with Mo-based cluster units as fundamental building blocks, the surface of this remarkably family of materials has been only barely scratched. Further combined experimental and theoretical studies on these compounds will likely lead to the discovery of efficient thermoelectric materials. Beyond the borders of thermoelectricity, the fact that cluster compounds are often prone to various lattice and electronic instabilities also makes studies of their low-temperature transport properties an important area of fundamental interest.

Accepted manuscript

5. References

- [1] H. J. Goldsmid *Thermoelectric Refrigeration*. Temple Press Books Ltd: London; 1964.
DOI:10.1007/978-1-4899-5723-8.
- [2] D. M. Rowe (ed.), *Thermoelectrics and its Energy Harvesting* (CRC Press, 2012).
- [3] G. Tan, L.-D. Zhao, M. G. Kanatzidis, *Chem. Rev.* 116, 12123 (2016).
- [4] S. R. Brown, S. M. Kauzlarich, F. Gascoin, G. J. Snyder, *Chem. Mater.* 18, 1873 (2006).
- [5] U. Aydemir, A. Zevalkink, A. Ormeci, Z. M. Gibbs, S. Bux, G. J. Snyder, *Chem. Mater.* 27, 1622 (2015).
- [6] B. R. Ortiz, P. Gorai, V. Stevanovic, E. S. Toberer, *Chem. Mater.* 29, 4523 (2017).
- [7] Z. Wu, J. Li, X. Li, M. Zhu, K. Wu, X. Tao, B.-B. Huang, S. Xia, *Chem. Mater.* 28, 6917 (2016).
- [8] H. Zhang, H. Borrmann, N. Oeschler, C. Candolfi, W. Schnelle, M. Schmidt, U. Burkhardt, M. Baitinger, J.-T. Zhao, Yu. Grin, *Inorg. Chem.* 50, 1250 (2011).
- [9] Q. Guo, A. Assoud, H. Kleinke, *Adv. Energy Mater.* 4, 1400348 (2014).
- [10] K. Suekuni, K. Tsuruta, T. Ariga, M. Koyano, *Appl. Phys. Express* 5, 051201 (2012).
- [11] X. Lu, D. T. Morelli, Y. Xia, F. Zhou, V. Ozolins, H. Chi, X. Zhou, C. Uher, *Adv. Energy Mater.* 3, 342 (2013).
- [12] C. Bourgès, Y. Bouyrie, A. R. Supka, R. Al Rahal Al Orabi, P. Lemoine, O. I. Lebedev, M. Ohta, K. Suekuni, V. Nassif, V. Hardy, R. Daou, Y. Miyazaki, M. Fornari, E. Guilmeau, *J. Am. Chem. Soc.* 140, 2186 (2018).

- [13] Y. Bouyrie, C. Candolfi, A. Dauscher, B. Malaman, B. Lenoir, *Chem. Mater.* 27, 8354 (2015).
- [14] S. Sassi, C. Candolfi, G. Delaizir, S. Migot, J. Ghanbaja, C. Gendarme, A. Dauscher, B. Malaman, B. Lenoir, *Inorg. Chem.* 57, 422 (2018).
- [15] R. Chevrel, M. Sergent, J. Prigent, *J. Solid State Chem.* 3, 515 (1971).
- [16] K. Yvon *Current Topics in Material Science*; E. Kaldis (ed.); North-Holland: Amsterdam, Vol. 3, p 53 (1979).
- [17] T. Caillat, J.-P. Fleurial, G. J. Snyder, *Solid State Sci.* 1, 535 (1999).
- [18] P. Gougeon, M. Potel, R. Gautier, *Inorg. Chem.* 43, 1257 (2004).
- [19] P. Gougeon, J. Padiou, J. Y. Lemarouille, M. Potel, M. Sergent, *J. Solid State Chem.* 51, 218 (1984).
- [20] P. Gougeon, M. Potel, J. Padiou, M. Sergent, *Mater. Res. Bull.* 22, 1087 (1987).
- [21] R. Gautier, S. Picard, P. Gougeon, M. Potel, *Mater. Res. Bull.* 34, 93 (1999).
- [22] P. Gougeon, M. Potel, M. Sergent, *Acta Crystallogr.* C45, 182 (1989).
- [23] P. Gougeon, M. Potel, M. Sergent, *Acta Crystallogr.* C45, 1413 (1989).
- [24] P. Gougeon, M. Potel, J. Padiou, M. Sergent, *Mater. Res. Bull.* 23, 453 (1988).
- [25] S. Picard, P. Gougeon, M. Potel, *Acta Crystallogr.* C53, 1519 (1997).
- [26] S. Picard, P. Gougeon, M. Potel, *Angew. Chem.* 38, 2034 (1999).
- [27] S. Picard, J.-Y. Saillard, P. Gougeon, H. P. Noël, M. Potel, *J. Solid State Chem.* 155, 417 (2000).
- [28] S. Picard, J.-F. Halet, P. Gougeon, M. Potel, *Inorg. Chem.* 38, 4422 (1999).
- [29] P. Gougeon, P. Gall, R. Gautier, M. Potel, *Acta Crystallogr.* C66, i67 (2010).

- [30] T. Zhou, B. Lenoir, M. Colin, A. Dauscher, R. Al Rahal Al Orabi, P. Gougeon, M. Potel, E. Guilmeau, *Appl. Phys. Lett.* 98, 162106 (2011).
- [31] T. Zhou, M. Colin, C. Candolfi, C. Boulanger, A. Dauscher, E. Santava, J. Hejtmanek, P. Baranek, R. Al Rahal Al Orabi, M. Potel, B. Fontaine, P. Gougeon, R. Gautier, B. Lenoir, *Chem. Mater.* 26, 4765 (2014).
- [32] R. Al Rahal Al Orabi, P. Gougeon, P. Gall, B. Fontaine, R. Gautier, M. Colin, C. Candolfi, A. Dauscher, J. Hejtmanek, B. Malaman, B. Lenoir, *Inorg. Chem.* 53, 11699 (2014).
- [33] P. Gougeon, P. Gall, R. Al Rahal Al Orabi, B. Fontaine, R. Gautier, M. Potel, T. Zhou, B. Lenoir, M. Colin, C. Candolfi, A. Dauscher, *Chem. Mater.* 24, 2899 (2012).
- [34] R. Al Rahal Al Orabi, B. Fontaine, R. Gautier, P. Gougeon, P. Gall, Y. Bouyrie, A. Dauscher, C. Candolfi, B. Lenoir, *Inorg. Chem.* 55, 6616 (2016).
- [35] G. Daigre, P. Gougeon, P. Gall, R. Gautier, O. Guillou-Viry, J.-B. Vaney, C. Candolfi, A. Dauscher, B. Lenoir, *J. Solid State Chem.* 237, 1–6 (2016).
- [36] P. Masschelein, C. Candolfi, A. Dauscher, C. Gendarme, R. Al Rahal Al Orabi, P. Gougeon, M. Potel, P. Gall, R. Gautier, B. Lenoir, *J. Alloys Compd* 739, 360 (2018).
- [37] M. Colin, T. Zhou, B. Lenoir, A. Dauscher, R. Al Rahal Al Orabi, P. Gougeon, M. Potel, P. Baranek, C. Semprinoschnig, *J. Electron. Mater.* 41, 1360 (2012).
- [38] P. Gougeon, P. Gall, O. Merdrignac-Conanec, L. Aranda, A. Dauscher, C. Candolfi, B. Lenoir, *Inorg. Chem.* 56, 9684 (2017).
- [39] R. Al Rahal Al Orabi, B. Boucher, B. Fontaine, P. Gall, C. Candolfi, B. Lenoir, P. Gougeon, J.-F. Halet, R. Gautier, *J. Mater. Chem. C* 5, 12097 (2017).

- [40] S. M. Butorin, K. O. Kvashnina, M. Klintonberg, M. Kavcic, M. Zitnik, K. Bucar, P. Gougeon, P. Gall, C. Candolfi, B. Lenoir, *ACS Appl. Energy Mater.* 1, 4032 (2018).
- [41] P. Gougeon, R. Al Rahal Al Orabi, B. Boucher, P. Gall, B. Fontaine, R. Gautier, A. Dauscher, C. Candolfi, B. Lenoir, to be published.
- [42] P. Gougeon, J. Padiou, J. Y. Le Marouille, M. Potel, M. Sergent, *J. Solid State Chem.* 51, 218 (1984).
- [43] P. Gougeon, M. Potel, R. Gautier, *Inorg. Chem.* 43, 1257 (2004).
- [44] A. Lipka, K. Yvon, *Acta Cryst. B* 36, 2123 (1980).
- [45] T. Hughbanks, R. Hoffmann, *J. Am. Chem. Soc.* 105, 1150 (1983).
- [46] R. Gautier, P. Gougeon, J.-F. Halet, M. Potel, J.-Y. Saillard, *J. Alloys Compd.* 262-263, 311 (1997).
- [47] D. Salloum, R. Gautier, P. Gougeon, M. Potel, *J. Solid State Chem.* 177, 1672 (2004).
- [48] D. Salloum, P. Gougeon, M. Potel, R. Gautier, *C. R. Chim.* 11-12, 1743 (2005).
- [49] G. A. Slack, D. W. Oliver, F. H. Horn, *Phys. Rev. B* 4, 1714 (1971).
- [50] G. A. Slack in *Semiconductors and Semimetals* (edited by F. Seitz, D. Turnbull and H. Ehrenreich, Academic Press, New York, 1979), p. 1, Vol. 34.
- [51] T. Mori, *Small* 13, 1702013 (2017).
- [52] Y. Bouyrie, C. Candolfi, S. Pailhès, M. M. Koza, B. Malaman, A. Dauscher, J. Tobola, O. Boisron, L. Saviot, B. Lenoir, *Phys. Chem. Chem. Phys.* 17, 19751 (2015).
- [53] W. Lai, Y. Wang, D. T. Morelli, X. Lu, *Adv. Funct. Mater.* 25, 3648 (2015).
- [54] M. D. Nielsen, V. Ozolins, J. P. Heremans, *Energy Environ. Sci.* 6, 570 (2013).
- [55] S. Lee, K. Esfarjani, T. Luo, J. Zhou, Z. Tian, G. Chen, *Nature Comm.* 5, 3525 (2014).

- [56] D. J. Safarik, A. Llobet, D. D. Byler, J. C. Lashley, J. R. O'Brien, N. R. Dilley, Phys. Rev. B, 85, 014103 (2012).
- [57] M. M. Koza, A. Leithe-Jasper, E. Sischka, W. Schnelle, H. Borrmann, H. Mutka, Yu. Grin, Phys. Chem. Chem. Phys. 16, 27119 (2014).
- [58] M. M. Koza, H. Mutka, Y. Okamoto, J.-I. Yamaura, Z. Hiroi, Phys. Chem. Chem. Phys. 17, 24837 (2015).
- [59] B. C. Chakoumakos, B. C. Sales, D. G. Mandrus, J. Alloys Compd. 322, 127 (2001).
- [60] S. Paschen, W. Carrillo-Cabrera, A. Bentien, V. H. Tran, M. Baenitz, Yu. Grin, F. Steglich, Phys. Rev. B 64, 214404 (2001).
- [61] J. Xu, J. Tang, K. Sato, Y. Tanabe, H. Miyasaka, M. Yamashita, S. Heguri, K. Tanigaki, Phys. Rev. B, 82, 085206 (2010).
- [62] K. Umeo, M. A. Avila, T. Sakata, K. Suekuni, T. J. Takabatake, Phys. Soc. Jpn. 74, 2145 (2005).
- [63] B. C. Sales, B. C. Chakoumakos, R. Jin, J. R. Thompson, D. Mandrus, Phys. Rev. B 63, 245113 (2001).